Geobiology

Geobiology (2012) DOI: 10.1111/j.1472-4669.2012.00334.x

# Cyanobacterial diversity and activity in modern conical microbialites

T. BOSAK,[1] B. LIANG,[1,2] T.-D. WU,[3,4] S. P. TEMPLER,[1,5] A. EVANS,[1] H. VALI,[6,7] J.-L. GUERQUIN-KERN,[3,4] V. KLEPAC-CERAJ,[8,9] M. S. SIM[1] AND J. MUI[6]

[1]*Department of Earth, Atmospheric and Planetary Sciences, Massachusetts Institute of Technology, Cambridge, MA, USA*
[2]*Institute of Earth Sciences, Nangang, Taipei, Taiwan*
[3]*INSERM, Orsay, France*
[4]*Laboratoire de Microscopie Ionique, Institut Curie, Orsay, France*
[5]*Roche Molecular Diagnostics, Basel, Switzerland,*
[6]*Facility for Electron Microscopy Research, McGill University, Montreal, QC, Canada*
[7]*Department of Anatomy and Cell Biology, McGill University, Montreal, QC, Canada*
[8]*The Forsyth Institute, Cambridge, MA, USA*
[9]*Department of Biological Sciences, Wellesley College, Wellesley, MA, USA*

## ABSTRACT

Modern conical microbialites are similar to some ancient conical stromatolites, but growth, behavior and diversity of cyanobacteria in modern conical microbialites remain poorly characterized. Here, we analyze the diversity of cyanobacterial 16S rRNA gene sequences in conical microbialites from 14 ponds fed by four thermal sources in Yellowstone National Park and compare cyanobacterial activity in the tips of cones and in the surrounding topographic lows (mats), respectively, by high-resolution mapping of labeled carbon. Cones and adjacent mats contain similar 16S rRNA gene sequences from genetically distinct clusters of filamentous, non-heterocystous cyanobacteria from Subsection III and unicellular cyanobacteria from Subsection I. These sequences vary among different ponds and between two sampling years, suggesting that coniform mats through time and space contain a number of cyanobacteria capable of vertical aggregation, filamentous cyanobacteria incapable of initiating cone formation and unicellular cyanobacteria. Unicellular cyanobacteria are more diverse in topographic lows, where some of these organisms respond to nutrient pulses more rapidly than thin filamentous cyanobacteria. The densest active cyanobacteria are found below the upper 50 μm of the cone tip, whereas cyanobacterial cells in mats are less dense, and are more commonly degraded or encrusted by silica. These spatial differences in cellular activity and density within macroscopic coniform mats imply a strong role for diffusion limitation in the development and the persistence of the conical shape. Similar mechanisms may have controlled the growth, morphology and persistence of small coniform stromatolites in shallow, quiet environments throughout geologic history.

Received 6 October 2011; accepted 30 April 2012

Corresponding author: T. Bosak. Tel.: +01-617-324-3959; fax: +01-617-253-8630; e-mail: tbosak@mit.edu

## INTRODUCTION

The macroscopic record of attached, laminated sedimentary rocks 'accretionary from a point or limited surface' (Semikhatov *et al.*, 1979) called stromatolites may record microbial interactions with sediments throughout Earth's sedimentary history (Grotzinger & Knoll, 1999). Stromatolites are conspicuous features in many Archean and Proterozoic carbonate strata, but the relationships between microscopic processes that build individual laminae and the preservable macroscopic shapes of stromatolites are not well understood. Evidence that microbial growth, movement and orientation influenced the formation of stromatolite laminae is particularly elusive in progressively older stromatolites owing to the abundance of precipitated cements and recrystallization (e.g., Hofmann & Jackson,

S.P.T., B.L., T.D.W. and T.B. contributed equally to this work.

1987; Kah & Knoll, 1996; Bartley *et al.*, 2000; Pope & Grotzinger, 2000). Small conical stromatolites and tufts as old as 3.0 billion years stand out as a biologically influenced end-member of precipitated stromatolites with modern, distinctly biogenic analogs that grow only in the presence of cyanobacteria (Fig. 1, Walter *et al.*, 1972, 1976; Grey, 1980; Beukes & Lowe, 1989; Buick, 1992; Jones *et al.*, 2002; Bosak *et al.*, 2009; Petroff *et al.*, 2010). Given these morphological similarities, one may ask whether similar factors have been responsible for the growth and persistence of coniform mats throughout geologic history. Here, we explore these factors by examining cyanobacterial diversity, biomass density and temporal changes in cyanobacterial communities in modern coniform microbialites from Yellowstone National Park (YNP, Figs 1 and 2).

Microscopic examinations of modern conical mats focus primarily on thin filamentous cyanobacteria. Walter *et al.* (1976) uses microscopy and laboratory enrichment cultures to identify filamentous cyanobacterium *Phormidium tenue* var. *granuliferum* as the principal cone-building organism. Variably lithified filaments morphologically similar to *P. tenue* also can be seen in cones from YNP and New Zealand (Cady & Farmer, 1996; Jones *et al.*, 2002), whereas unicellular organisms and *Pseudoanabaena* are more commonly observed in the surrounding mats (Walter *et al.*, 1976). The true molecular, morphological and functional diversity of cyanobacteria in coniform mats likely exceeds these microscopic estimates. Even before the advent of molecular techniques, Weller *et al.* (1975) reported the formation of cones in a number of axenic cyanobacterial cultures but did not describe any phenotypic or morphological differences among these cultures. Recent molecular studies show the presence of multiple genetically distinct cyanobacteria in photosynthetic mats from hot springs (Ferris *et al.*, 2003; Lacap *et al.*, 2005, 2007; Lau *et al.*, 2005; Ward *et al.*, 2006; McGregor & Rasmussen, 2008; Boomer *et al.*, 2009; Foster *et al.*, 2009). A single study (Lau *et al.*, 2005) analyzed the cyanobacterial diversity in cones, ridged cones and flat-topped cones from one of the outflows of Black Sands Pool in YNP and reported six cyanobacterial sequences in all cones: one *Phormidium*-like sequence, a sequence similar to unicellular *Synechococcus*, and four sequences with the closest similarity to uncultured cyanobacteria. Because the mats around cones contained only *Synechococcus*-like sequences that were distinct from those in cones, these authors suggested that cones and mats, as distinct components of coniform mats, contained different microbial assemblages (Lau *et al.*, 2005).

It remains unclear how to marry the reported molecular diversity of cyanobacteria in coniform mats with microscopic

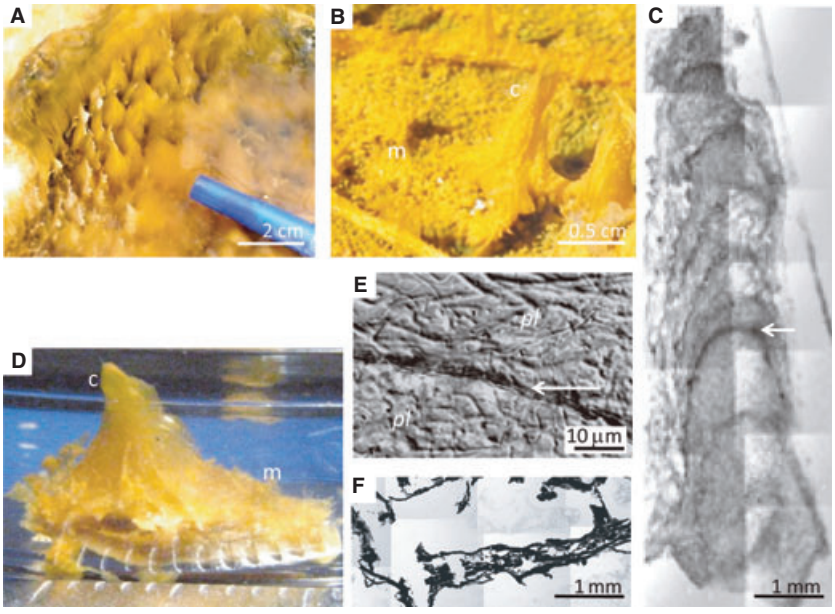


**Fig. 1** Coniform mats in alkaline hot springs in Yellowstone National Park (YNP) (A, B) Photographs of coniform mats in small depressions and quiet ponds. (A) Dense cones. (B) Coniform mat consisting of cones (c) and surrounding mats (m). (C) Transmitted light micrograph of a vertical 30-µm-thick section through a cone showing thin dark laminae (arrow) and thick, porous laminae. Arrow points to the region magnified in (E). (D) Photograph of a YNP cone and the adjacent mat used in the 30-min labeling experiment. A similar cone was used in the 60-min incubation. Small divisions on the scale are 1 mm long. (E) Transmitted light micrograph of the vertical section of a cone showing aligned filaments in a thin lamina (arrow) and randomly oriented filaments in the porous laminae *pl*. (F) Transmitted light micrograph of the vertical section through the mat showing heavily lithified thin laminae (dark, Si grains) and empty regions. The presence of Si was confirmed by energy-dispersive X-ray spectroscopy.

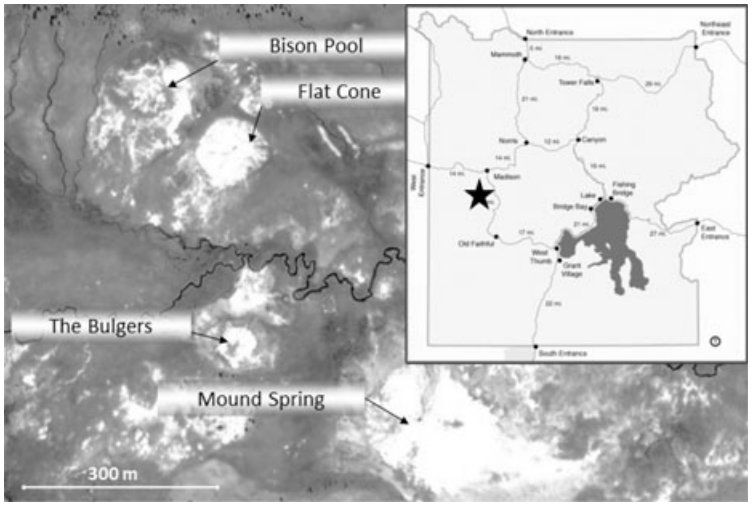


**Fig. 2** Map of the sampling area (Sentinel Meadows, Yellowstone National Park) created by Google Maps, © Google. Inset on the right contains the map of Yellowstone National Park created by Google Maps. Star in the inset indicates the sampling area.

observations. Namely, filamentous cyanobacteria are commonly seen in mats (e.g., Walter *et al.*, 1976), but only sequences similar to unicellular *Synechococcus* are reported from the mats around cones (Lau *et al.*, 2005). It also remains unclear whether only one organism drives the formation of coniform mats in YNP, or whether these structures contain multiple genetically distinct organisms capable of vertical aggregation. Here, we address these questions by:

- analyzing the diversity of cyanobacteria in cones and mats in multiple ponds around four different hot springs
- characterizing the ability of different cyanobacteria to form vertical structures in laboratory enrichment cultures
- measuring the activities and the densities of cells at the topographic highs and lows of natural coniform mats in YNP.

Our findings reveal that modern coniform mats contain multiple, genetically distinct filamentous and unicellular cyanobacteria and that these cyanobacterial communities vary in space and time, contributing to the interannual persistence of coniform structures. At any given point in time, the growth, degradation and lithification of microbes in coniform mats depend on the position within the three-dimensional topography.

## MATERIALS AND METHODS

### Sample collection

Samples of conical stromatolites used in laboratory enrichments, field incubations with labeled carbon, microscopic analyses and a subset of molecular analyses were collected in one pond of Mound Spring in YNP in September 2008. Cones that were incubated with labeled carbon were not used in molecular analyses, but adjacent cones from the same pond were sampled and analyzed instead. Most samples for comparative molecular analyses were collected in August 2009 as pairs of cones and adjacent mats (Fig. 1B, D) from 14 ponds fed by the outflow channels of four different hot springs in the Sentinel Meadows thermal area: Mound Spring, Flat Cone Spring, Bison Pool, and the Bulgers (Table 1, Fig. 2). Some of these samples were also analyzed by transmitted electron microscopy (TEM, Fig. 3D). All field incubations and sample collections were performed under permit (#YELL-2008-SCI-5758 for the sampling of coniform mats in Sentinel Meadows and Fairy Creek). All samples were excised in duplicates by a sterile surgical blade and placed in sterile Eppendorf tubes, stored on dry ice during field collection and transport, and stored at −80 °C in the laboratory. Flow in ponds in 2009 was monitored by placing the floating lid of a 15-mL BD FalconTM tube (BD Biosciences, San Jose, CA, USA) on the surface of the liquid and measuring the distance that the lid travelled in time.

### Light and epifluorescence microscopy

Samples were fixed with 2.5% glutaraldehyde in 0.1 M sodium cacodylate buffer (pH 7.4) for 2 h. Buffer-washed samples were embedded in Sakura TissueTek O.C.T. compound (VWR, West Chester, PA, USA), frozen for at least 2 h and sectioned to a thickness of 10–30 μm using a cryo-stat (Leica, Wetzlar, Germany). Thin sections were washed with buffer and imaged using an Axio Imager M1 epifluorescence microscope (Carl Zeiss, Thornwood, NY, USA) with differential interference contrast and phase contrast modules. LSM510 confocal microscope with quasar spectral detection (Carl Zeiss) was used to distinguish

**Table 1** Conditions at sampling sites around four Yellowstone National Park (YNP) alkaline hot springs in Sentinel Meadows (Fig. 2). The sampling sites were defined by the appearance of coniform mats. Only one pond was sampled in Flat Cone because other coniform structures there were permanently exposed

| Hot spring | General description | pH at source | pH range in sampled area | *T* at source (°C) | *T* range (°C) in sampled area | No. of sampled ponds | No. of samples |
|---|---|---|---|---|---|---|---|
| Mound Spring 2008 | Slightly elevated spring with single, boiling rimmed source (approximately 2 m in diameter) and two major outflow channels. High water level in ponds; coniform mats permanently submerged. | na | 8.67–9.20 | na | 42.1–43.6 | 1 | 5 |
| Mound spring 2009 | Slightly elevated spring with single, boiling rimmed source (approximately 2 m in diameter) and two major outflow channels. Sampling starts approximately 10 m away from source. Low water level in ponds; coniform mats covered by a thin film of water. | 9.24 | 9.26–9.57 | 78.2 | 24.7–51.3 | 6 | 13 |
| The Bulgers 2009 | Flat spring with two small boiling sources (each approximately 0.5 m in diameter) and two major outflow channels. Sampling starts approximately 5 m away from source. Low water level in ponds; coniform mats covered by a thin film of water. | 8.30 | 8.50–9.00 | 86.4 | 32.0–42.1 | 5 | 12 |
| Flat Cone spring 2009 | Elevated spring with single, non-boiling rimmed source (approximately 1.5 m in diameter) and one major outflow channel. Source erupted occasionally. Between eruption cycles, most ponds at minimal water level. Coniform mats exposed in most ponds. | 8.78 | 9.20–9.30 | 70.0 | 22.2 | 1 | 4 |
| Bison spring 2009 | Flat spring with single, non-boiling source (approximately 1.5 m in diameter) and one major outflow channel. Coniform mats under 5–10 cm of water. | 8.00 | 8.50–8.90 | 88.5 | 33.8–47.4 | 2 | 4 |

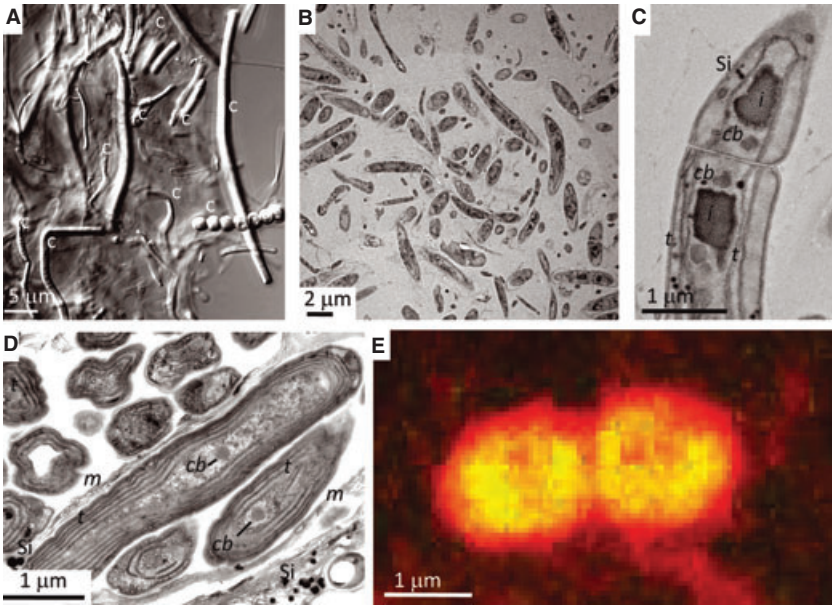


**Fig. 3** Morphology, ultrastructure and fluorescence of filamentous cyanobacteria in cones. (A) Differential interference contrast micrograph of cells in the cone tip. *c* denotes representative cyanobacterial morphologies identified by chlorophyll autofluorescence. The beaded morphology is rare, other morphologies are common. (B) Transmission electron microscopy (TEM) image of cells in the tip of a Yellowstone National Park (YNP) cone showing many different cross-sections of approximately 1-µm-wide filaments. (C) TEM image of a typical filamentous spear-tipped cyanobacterium in the tip of a cone. The cell contains inclusion bodies *i*, carboxysomes *cb*, thylakoids *t*, and $SiO_2$ granules *Si* (less frequent). This cone was collected in 2008 and was not incubated with labeled carbon. (D) TEM image of a typical sausage-shaped cyanobacterium surrounded by mucilage *m* and silica granules *Si*. This sample shows the tip of a cone collected in 2009. (E) Confocal fluorescence micrograph of typical *Synechococcus*-like cyanobacteria that occur rarely on the surface of cones, but are more common in the mat. Orange autofluorescence is consistent with the presence of phycoerhythrin. Chlorophyll *a* autofluoresces red.

between chlorophyll autofluorescence (CY3 filter, excitation 558 nm and emission 568 nm) and the orange autofluorescence of phycoerythrin (FITC filter, excitation 490 nm and emission 520 nm).

### Genomic DNA extraction

Genomic DNA from approximately 0.5 g of all samples was extracted using UltraClean soil DNA isolation kit

(Mo Bio Laboratories, Carlsbad, CA, USA) following the manufacturer's protocol for maximum yield. The concentrations of DNA were measured using a NanoDrop 1000 (Thermo Fisher Scientific Inc., Wilmington, DE, USA).

### PCR conditions

Universal bacterial primers 27F (5′-AGAGTTTGAT CATGGCTCAG-3′) and 1492R (5′-TACGG(C/T)TAC-CTTGTTACGACTT-3′) (Lane, 1991) were used to amplify bacterial 16S rRNA genes. Amplification used an initial denaturation step at 95 °C for 4 min, followed by 30 cycles of denaturation at 95 °C for 35 s, annealing at 52 °C for 55 s, elongation at 72 °C for 55 s, and a final 3 min elongation step at 72 °C in a MyCyclerTM Thermal Cycler (Bio-Rad, Hercules, CA, USA). PCR mixtures contained (per 50 μL): 0.4 μM of primers, 2 μL of DNA template (or 2 μL of purified 16S rRNAgene PCR product), 1× Ex TaqTM buffer (Takara Bio Inc., Shiga, Japan), 2 mM $MgCl_2$, 1.25 U TaKaRa ExTaqTM (Takara Bio Inc.), 0.25 mM of each dNTP. The PCR products were purified using the QIAquick PCR Purification Kit (Qiagen Inc., Valencia, CA, USA) and re-amplified in a nested PCR using primers specific to cyanobacteria: forward primer 359F (GGG GAA TYT TCC GCA ATG GG) with a GC clamp (CGC CCG CCG CGC CCC GCG CCG GTC CCG CCG CCC CCG CCC G) and an equimolar mixture of reverse primer 781R(a) (GAC TAC TGG GGT ATC TAA TCC CAT T) and 781R(b) (GAC TAC AGG GGT ATC TAA TCC CTT T) (Nubel *et al.*, 1997; Lau *et al.*, 2005). For the amplification using cyanobacteria-specific primers, amplification conditions were as follows: initial denaturation step at 94 °C for 1 min 25 s; followed by 13 cycles of denaturation for 35 s at 95 °C, primer annealing for 55 s at 55 °C and extension for 45 s at 72 °C; 13 cycles with 2 min extension time followed by nine cycles with a 3-min extension; and a final 10-min extension at 72 °C, as previously described (Lau *et al.*, 2005). PCR mixtures contained (per 50 μL): 0.4 μM of primers, 2 μL of purified 16S rRNAgene PCR product), 1 × Ex TaqTM buffer (Takara Bio Inc.), 1.5 mM MgCl2, 1.25 U TaKaRa ExTaqTM (Takara Bio Inc.), 0.25 mM each dNTP. The PCR products were purified using the QIAquick PCR Purification Kit (Qiagen Inc.).

### Denaturing gradient gel electrophoresis

Approximately, 300–500 ng of amplicons from the nested PCR were separated using a denaturing gradient gel electrophoresis (DGGE) System (C.B.S. Scientific, Del Mar, CA, USA) on a gel (0.75 mm thick, 15 cm × 20 cm) by applying a double gradient of 7.5% to 12% (w/v) polyacrylamide and between 20% and 60% of denaturant [100% denaturant equals 7 M urea and 40% (v/v) formamide]. Electrophoresis was carried out at 150 V for 13.5 h at 60 °C in 1× TAE buffer. Polyacrylamide gels were stained with SYBR™ Gold nucleic acid gel stain (Invitrogen, Carlsbad, CA, USA) and imaged using Quantity One 4.2 software to detect separated amplifications products (bands) in the DGGE gels. Individual DGGE bands were excised and rinsed in 100 μL sterile nuclease-free molecular grade water for 30 min. These gel plugs were used as template DNA in a PCR reaction using cyanobacteria-specific primers 359F and an equimolar mixture of reverse primers 781R(a) and 781(b) using the amplification conditions described previously. PCR products were re-analyzed by DGGE to confirm single-band recovery, excised from the gel and purified with the QIAquick PCR Purification Kit (Qiagen) prior to sequencing.

### Phylogenetic and occurrence data analyses

Sequences were compared with sequences deposited in GenBank using the Basic Local Alignment Search Tool (BLAST-N) to determine the nearest relatives and percent similarity (Altschul *et al.*, 1997). All sequences were checked for the presence of chimeras using Bellerophon (Huber *et al.*, 2004), accessed through the Greengenes portal (DeSantis *et al.*, 2006a). Sequences retrieved from excised DGGE bands were grouped into 97% sequence identity clusters and are referred to as operational taxonomic units (OTUs). Cyanobacterial OTUs were classified taxonomically according to Castenholz (2001).

Partial sequences were aligned using Greengenes' NAST alignment tool and imported into Greengenes May 2007 ARB database (DeSantis *et al.*, 2006a,b) using ARB software package (http://arb-home.de; Ludwig *et al.*, 2004). Affiliations of partial sequences were confirmed by the addition to a Greengenes CoreSet tree consisting of full-length sequences, without changing branch topology using the parsimony insertion tool in ARB. The filter 'lanemaskPH' was used to ignore hypervariable regions of the 16S rRNA molecule provided with the ARB database. The phylogenetic tree was constructed by using maximum likelihood method RAxML-VI-HPC under the GTRCAT model of evolution (Stamatakis *et al.*, 2008). The robustness of inferred tree topologies was evaluated by bootstrap analysis using 1000 replicates. *Aquifex aeolicus*, str. VF5 was used as an outgroup and was subsequently pruned from the tree.

To analyze the occurrence of various OTUs in samples from different ponds and hot springs, UPGMA hierarchical clustering analysis was performed with average linkage, and Jaccard distance (Legendre & Legendre, 1998) using the hierarchy module of the SciPy package (v. 0.9.0) of the Python programming language (Jones *et al.*, 2001). To

identify cone- or mat-specific OTUs, the statistical significance of the association of OTUs with morphology or temperature was assessed separately for each OTU using a two-sided Fisher's exact test (Agresti, 1990), as implemented in the statistical package of the R programming language (v. 2.11.0), www.r-project.org. In this analysis, temperature values were discretized to 'hot' ($\geq$30 °C) or 'cold' (<30 °C). Additionally, the dependence of the distribution of OTUs on continuous temperature values was assessed using logistic regression. Linear logistic regression was also used to test the dependence of distribution of OTUs on temperature. Dendrograms were generated using UPGMA with average linkage.

### Measurements of photosynthetic rates

Oxygen concentrations and photosynthetic rates were determined using a Clark-type oxygen microsensor (OX-25 and OX-50; Unisense, Aarhus, Denmark) with a guard cathode (Revsbech, 1989). Linear calibration of microsensors was performed using air-saturated and anoxic pond water. The diffusive flux of oxygen was calculated from steady state oxygen microprofile using Fick's first law of one-dimensional diffusion (Jorgensen & Revsbech, 1985):

$$J_z = \mathrm{De} \cdot \mathrm{d}C_z/\mathrm{d}_z,$$

where De is an effective diffusion coefficient and $dC_z/d_z$ is the slope of the microprofile at death z, De in the bacterial colony was assumed to be $2.0 \times 10^{-5}$ $cm^2$ $s^{-1}$ (Lassen *et al.*, 1998; Grotzschel & de Beer, 2002). Net photosynthetic rates in individual layers were determined from the balance between oxygen fluxes through the overlying and underlying areas. The gross photosynthetic rate was measured using oxygen microelectrodes and the light/dark shift method (Revsbech & Jorgensen, 1983).

### Enrichment cultures

Castenholz-D (Castenholz, 1988) agar plates (2%) were scored with parallel lines using dry calcium alginate swabs (Burton & Lee, 1978; Vaara *et al.*, 1979), inocula from Mound Spring 2008 were placed at the beginning of each scored line and incubated for approximately 24 h at 45 °C in a light gradient (from 13.9 to 12.8 μm photons $m^{-2}$) to enrich for phototactic, gliding cyanobacteria. The migration of filaments was monitored by epifluorescence microscopy as described previously. Single filaments that had glided along the scored path were excised by a sterile surgical blade and cultured in modified liquid Castenholz-D medium at pH 8 (Bosak *et al.*, 2009) containing autoclaved silica sand (VWR International, Radnor, PA, USA). This process was repeated 25 times. The liquid cultures were grown with a fluorescent cold light source with a 12-h day, 12-h night cycle and the medium was exchanged periodically. The purity of cultures was tested by plating the culture onto 100% LB, 10% LB, and glucose/fructose (5 mM final concentration) agar plates, microscopically, and by the amplification of a single 16S rRNA gene from biofilms grown in the liquid medium using universal bacterial primers 27F (5′-AGA GTT TGA TCA TGG CTC AG-3′) and 1492R (5′-TAC GG(C/T) TAC CTT GTT ACG ACT T-3′) (Lane, 1991). The resulting enrichments were characterized by microscopy and by a series of growth experiments at various light intensities that encompassed measurements of chlorophyll A and visual characterization of cyanobacterial aggregation. Cyanobacteria enriched by this process are described in Figs 5 and 6 as XAN-1, 8, 12, and FYG.

### Carbon isotope labeling

Individual cones and approximately 1 cm wide surrounding mats (as shown in Fig. 1D) were labeled in YNP using a modified Castenholz-D medium (Castenholz, 1988; Bosak *et al.*, 2009) amended with sodium bicarbonate-$^{13}C$ (98 atom%, Isotec, Inc., Miamisburg, Ohio). The total $H^{13}CO_3^-$ was 2.58 mM per labeling in 100 mL of the incubation medium. All samples were incubated in YNP from 1 to 2 pm at ambient light intensity of approximately 1500 μE $m^{-2}$ $s^{-1}$, in the host spring at ambient pond temperature (42 °C).

### Transmission electron microscopy (TEM)

Isotopically labeled and unlabeled control samples were fixed by 2.5% glutaraldehyde in 0.1 M sodium cacodylate buffer (pH 7.4), washed with buffer, and post-fixed in 1% osmium tetroxide and 1.5% potassium ferrocyanide. The fixed samples were dehydrated through a gradient series (30–100%) of acetone/water solutions and embedded in epoxy resin (Epon). Ultrathin sections (70–100 nm) and semi-thin sections (approximately 500 nm) were cut from the resin blocks by using a Reichert-Jung Ultracut E ultramicrotome (Reichert-Jung AG, Vienna, Austria) with a Diatome diamond knife (Diatome AG, Biel, Switzerland). The ultrathin sections were transferred onto 200-mesh Cu TEM grids with Formvar-carbon support film for NanoSIMS-TEM correlation imaging. TEM was performed by a FEI Tecnai 12 TEM (FEI Company, Eindhoven, the Netherlands) equipped with a Gatan Bioscan CCD camera Model 792 (Gatan, Inc., Pleasanton, CA, USA). An accelerating voltage of 120 kV was applied in bright-field mode.

### Secondary ion mass spectrometry (NanoSIMS) mapping

Secondary ion mass spectroscopy (SIMS) imaging was performed using a NanoSIMS-50 Ion Microprobe (Cameca,

Gennevillieres, France) operating in scanning mode. The semi-thin sections (approximately 500 nm) were cut at the same time as the ultrathin sections for observation in TEM, providing complementary chemical information by SIMS to the high spatial resolution structural information by TEM.

A tightly focused, high-energy primary ion beam of $Cs^+$ bombards the sample surface and generates negative secondary ions during the collision cascade. These secondary ions are directed to a magnetic mass spectrometer that ensures high transmission with a high mass resolution. The parallel detection system allows the simultaneous recording of up to five ion species, permitting reliable comparisons between different ions, especially between isotopic ions from the same microvolume. The primary beam, operated in probe scanning mode, steps over the surface of the sample to create images of the selected ion species. In our study, survey mosaic secondary ion images were generated as 256 × 256 pixel rasters of 60 μm × 60 μm pixels, with the probe intensity of 5 pA and a typical probe size of 150 nm. To obtain high-resolution images of intracellular details, the raster was reduced to 15–30 μm, with the probe size smaller than 100 nm and an intensity of about 1 pA. Images were created for the following: $^{12}C^-$, $^{13}C^-$, $^{12}C^{14}N^-$, $^{13}C^{14}N^-$ and $^{32}S^-$. Figures S2 and S3 provide examples of survey mosaic images and position-dependent high-resolution scans. The dwell time per pixel was 15 ms for survey images and 30 ms for high-resolution images. High mass resolution separated $^{13}C^{14}N^-$ from the isobaric $^{12}C^{15}N^-$ species (Guerquin-Kern *et al.*, 2005) and prevented the mass interference from $^{11}B^{16}O^-$ species. Compared with ion species $^{12}C^-$ and $^{13}C^-$, $^{12}C^{14}N^-$ and $^{13}C^{14}N^-$ have higher intensities and are therefore both more statistically reliable and better able to indicate carbon associated with biomass. Thus, the ratio (%) of $^{13}C^{14}N^-/^{12}C^{14}N^-$ was used to track the relative carbon uptake (enrichment). Color ratio images were generated in OpenMIMS, an ImageJ (Rasband, 1997–2006) plugin developed by Claude Lechene's Laboratory. OpenMIMS allows the visualization of ratio value in a HSI (Hue-Saturation-Intensity) image (Benson, 2003; Poczatek *et al.*, 2009).

To calculate the average $^{13}C^{14}N^-/^{12}C^{14}N^-$ ratio in the cells in each 60 μm × 60 μm survey image, the information pertaining to the microbial biomass (enriched in $^{13}C$) has to be distinguished from the background resin (natural $^{13}C$ abundance). The biomass has a much higher $CN^-$ ion signal than the resin, allowing the generation of a mask by adjusting the threshold level on the sum image of $^{13}CN^-$ and $^{12}CN^-$. The pixels in the resulting binary mask image have values of 1 or 0, corresponding to areas with and without cellular biomass, respectively. The total number of pixels with the value of 1 in the binary mask image was used as a measure of total cellular biomass. This binary mask image was multiplied by the measured $^{13}CN^-/^{12}CN^-$ ratio image to generate a $^{13}CN^-/^{12}CN^-$ ratio map, which eliminated the resin background. This biomass ratio map was used to calculate the net carbon uptake: the ratio characteristic for the unlabeled controls ($N = 3$, numerical value 1.25%) was first subtracted from each pixel value, and pixel values in thus corrected ratio of $^{13}CN^-/^{12}CN^-$ were integrated over the entire $^{13}CN^-/^{12}CN^-$ ratio map. To calculate the $^{13}C$ enrichment in individual filaments, we manually outlined individual filaments in the biomass ratio map and integrated the pixel values within the outlined area (ROI, region of interest) after the subtraction of the unlabeled control value (1.25%). Only distinctly filamentous cells were selected for this analysis to avoid bias caused by the random truncation during sectioning.

## RESULTS

### Environmental parameters at sampling sites

Coniform mats in YNP form in quiet ponds and other surface depressions where the flow is low (such as buffalo steps) and the pH is alkaline (pH > 8) (Fig. 1A,B, Table 1). The water level in the outflow channels in 2009 was low, periodically exposing some mats and covering others by only a thin film of water (Table 1). The temperature of the water around sampled coniform mats varied from 22.0 to 51.3 °C (Tables 1 and 2) and the flow on the surface was detectable only in two ponds in Mound Spring (44.6 and 55.3 °C). Coniform mats around Mound Spring in September 2008 were submerged under 2–4 cm of warm water (40–45 °C).

### Morphology and ultrastructure of cyanobacteria in cones and mats

Filaments in the dense thin laminae of cones were nearly parallel to the growth surface (Fig. 1C,E), whereas those in the porous thick laminae were sparsely distributed and randomly oriented with respect to the growth surface (Fig. 1C,E). Thick, porous laminae were rare or absent from the more heavily lithified adjacent horizontal mats (Fig. 1F), where many degraded cells and cells encrusted by silica were present (Figs S1–S3).

Cones sampled in 2008 contained various morphologically distinct cells that exhibited chlorophyll *a* autofluorescence (Fig. 3A), as well as <0.8-μm-thick filaments similar to those of *Roseiflexus*- and *Chloroflexus*-like organisms (Figs 3A and S4; Pierson & Castenholz, 1974; Pierson *et al.*, 1985; Hanada *et al.*, 2002). The most abundant cyanobacteria in the thin and thick laminae of cones were >100-μm-long filaments composed of 0.8–1 μm wide and 2–3-μm-long rectangular cells. These cells contain 3–4

**Table 2** Distribution of operational taxonomic units (OTUs) in the ponds of Mound Spring (MS), the Bulgers (BG), Bison Spring (BS), and Flat Cone (FC)

| OTU cluster | OTU | Number of ponds in each spring where OTU was present | OTU temperature range (°C) |
|---|---|---|---|
| Subsection III filamentous, non-heterocystous | 1 | MS(5), BG(3), BS(1) | 30.0–44.6 |
| | 2 | BG(5) | 30.0–42.1 |
| | 3 | MS(4) | 32.5–51.3 |
| | 4, 9, 29 | FC(1) | 22.2 |
| | 5 | BS(1) | 35.4 |
| | 18 | MS(6), BG(5), BS(2), FC(1) | 22.2–51.3 |
| | 32 | MS(6), BG(5), BS(1), FC(1) | 22.2–51.3 |
| | 19 | MS(3), BG(4), BS(2), FC(1) | 22.2–47.4 |
| | 20, 21,23,24 | MS(6), BG(5), BS(2), FC(1) | 22.2–47.4 |
| | 22 | MS(5), BG(4), BS(2), FC(1) | 22.2–47.4 |
| | 28 | BS(2) | 35.4–47.4 |
| | 30 | BS(1) | 35.4 |
| | 31 | MS(3) | 32.5–51.3 |
| Subsection I *Synechocystis*-like | 7 | MS(5), BG(1), FC(1) | 22.2–51.3 |
| | 8 | BG(1) | 30.0 |
| Subsection I *Synechococcus*-like | 10, 13, 15, 16 | BG(1) | 30.0 |
| | 11 | MS(5), BG(3), BS(2), FC(1) | 22.2–51.3 |
| | 12 | MS(6) | 32.5–51.3 |
| | 14 | MS(1) | 36.2–40.2 |
| | 17 | MS(1) | 32.5 |
| | 25 | MS(4) | 34.0–51.3 |
| | 26 | BG(3) | 30.0–42.1 |
| | 27 | MS(1) | 40.2–51.3 |
| Other (Acidobacteria) | 6 | MS(5), BG(4), BS(1), FC(1) | 22.2–51.3 |

peripherally arranged thylakoids, approximately 150–750-nm-wide subterminal granules (Nash, 1938) and cell walls that were commonly surrounded by fibrous mucilage. The terminal cells in some filaments were spear shaped (Figs 3C and 4A). These cells were less common in the tips of cones from Mound Spring that were sampled in 2009. YNP cones from 2008 and 2009 also contained sausage-shaped 0.9–1.2-μm-wide and 3–5-μm-long cells with 3–4 peripherally arranged thylakoids, intracellular granules (150–300 nm in diameter) and cell walls surrounded by fibrous mucilage (Fig. 3D). These sausage-shaped cyanobacteria, similar to *Synechococcus* sp. (e.g., Jones *et al.*, 1998; Cannon *et al.*, 2001; Castenholz, 2001), were very abundant in the intermittently exposed tips of cones from 2009 (Fig. 3D), and rare in the tips of permanently submerged cones from 2008. The silicification of the sticky matrix between these cells in cone tips (Fig. 3D) was likely promoted by the evaporation in the thin film of water or during periodic exposure (Table 1), but was still less heavy than the silicification in mats sampled in 2008. The approximately 0.8-μm-wide filaments and the 1 × 3 μm, sausage-shaped cells actively took up inorganic carbon (Fig. 4) and lacked the orange autofluorescence of phycoerythrin. This autofluorescence was instead observed within some relatively rare, 2-μm-wide oval cyanobacteria morphologically similar to *Synechococcus* (Fig. 3E). These oval or round cyanobacteria occurred only individually in cones, primarily on the very surface, but were more common in the adjacent topographic lows (Figs 4C,D and S2). Numerous ghosts of lysed cells and silica-encrusted cells were present in the topographic lows (Figs 1 and S1–S3). More extensive degradation of cells in mats also was reported by Walter *et al.* (1976).

### Molecular diversity of cyanobacteria in cones and mats

Sequences of cyanobacterial 16S rRNA genes in field samples of coniform mats from four different thermal features and from two different years attested to the contribution of a number of genetically distinct cyanobacteria to the construction and the interannual persistence of modern conical stromatolites (Fig. 5). The 33 samples from 2009, each consisting of a cone and the adjacent mat, contained a total of 18 different operational taxonomic units (OTUs) forming two clusters similar to filamentous *Leptolyngbya* (Fig. 5). Also present were 13 OTUs similar to the 16S rRNA genes of cyanobacteria from cultured representatives of *Synechocystis* and *Synechococcus* genera (Fig. 5). The PCR amplification method using primers specific to cyanobacteria also detected an unaffiliated OTU (OTU 6) similar to candidate division SR1 (Fig. 5, Davis *et al.*, 2009) and Acidobacteria (not included in the phylogenetic tree).

Table 2 summarizes the observed distribution of OTUs in the sampled ponds. More detailed description of the occurrences with respect to individual ponds, temperatures and morphologies (cones or mats) also can be seen in Figs

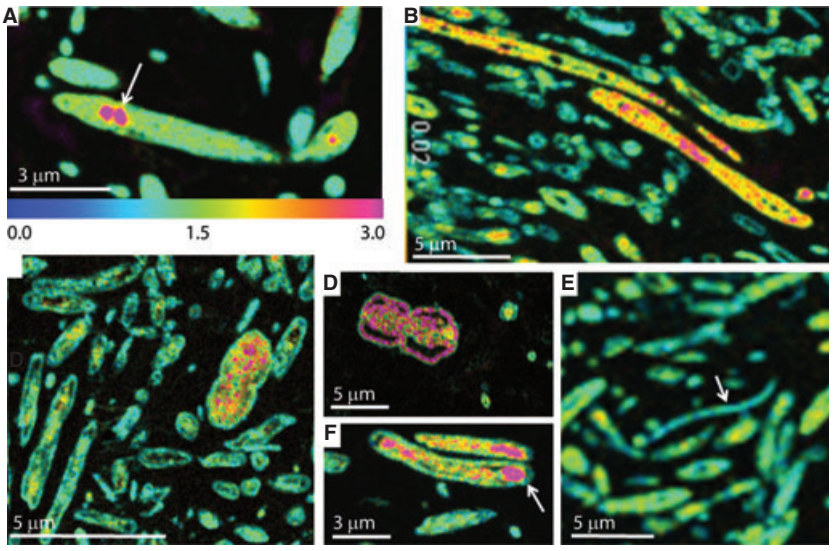


**Fig. 4** Carbon uptake by cells in Yellowstone National Park (YNP) cones and mats mapped as $^{13}CN^{-}/^{12}CN^{-}$. All samples were collected and incubated with labeled carbon in 2008. Relative enrichment levels above the 1.25% threshold abundance in all panels are shown on the same HSI color scale. (A) High-resolution map of a typical spear-tipped cell from the tip of a YNP cone incubated for 30 min. Arrow points to granules with a high $^{13}CN/^{12}CN^{-}$ ratio. (B) High-resolution map of typical filamentous cells approximately 150 μm below the tip of a YNP cone incubated for 60 min. (C) High-resolution map of an oval *Synechococcus*-like cell below the upper 0.3 mm of the YNP mat incubated for 30 min. Cells with this morphology, also shown in Fig. 3(E), are not abundant. (D) High-resolution map of a large oval cell from the YNP mat incubated for 60 min. This morphology occurs sporadically. (E) An unlabeled long thin filament (arrow) from a YNP cone incubated for 60 min (enlarged from a lower resolution map, see Materials and Methods). This filament is similar to the thinnest filaments in Fig. 3A. See Fig. S4 for more examples of this morphology and its carbon uptake. (F) High-resolution map of typical sausage-shaped cells approximately 320 μm below the tip of a cone incubated for 60 min. Arrow points to granules with a high $^{13}CN/^{12}CN^{-}$.

S5 and S6. Cones contained 2–10 OTUs from cyanobacterial Subsection III ('filamentous, non-heterocystous'; Castenholz, 2001) and 0–3 of the 'unicellular' *Synechococcus*- or *Synechocystis*-like OTUs from Subsection I (Castenholz, 2001), whereas the adjacent mats contained 0–5 OTUs from Subsection III and 0–5 unicellular OTUs (Fig. S6). Eight OTUs from the larger *Leptolyngbya*-like Subsection III cluster, (OTU 18–24, 32), occurred in samples from all hot springs (Table 2). Two of these ubiquitous OTUs (19, 22) occurred primarily in cones ($P = 0.0001$, Fisher's exact test, Fig. S6) and four (20, 21, 23, 24) almost always occurred together in cones and mats (Fig. S5, Jaccard similarity indices higher than 0.7). In fact, the presence or absence of these four OTUs defined the two major spatial clusters of cyanobacterial diversity (Fig. S5). The larger Subsection III cluster also contained sequences that were detected only around individual hot springs (Table 2). Various motile filamentous cyanobacteria from our laboratory enrichment cultures grouped with this cluster. Some cyanobacteria in these laboratory enrichment cultures (XAN-1 and XAN-12) formed cones under all growth conditions, while others (XAN-8) did not (Fig. 6). Also present in nearly all ponds was a sequence (OTU 1) from the smaller Subsection III cluster (Fig. 5, Table 2) that occurred primarily in cones ($P = 0.001$, Fig. S6). This sequence was similar to a filamentous cyanobacterium forming porous tubes and films in our laboratory enrichment cultures (FYG, Figs 5 and 6), and to the only OTU from Subsection III that was detected in coniform mats around Black Sands Pool (Lau *et al.*, 2005). Other sequences from this cluster (OTU 2, 3, 9) were detected both in mats and in cones, but only in individual hot springs (Table 2, Fig. S5).

Operational taxonomic units similar to 16S rRNA gene sequences of unicellular cyanobacteria were absent from more than 50% of the cones from 2009, but were detectable in 75% of the mats (all data shown in Fig. S6). These OTUs varied spatially, with only two detected in more than one spring (OTU 7, 11) and eight detected only in single samples of mats or cones (Table 2, Fig. S5). OTU 11, exhibiting the highest similarity to *Synechococcus* C9 and to a sequence previously reported in the mats surrounding YNP cones (Lau *et al.*, 2005; Fig. 5), was detected primarily in mats ($P = 0.0001$, Fig. S6). OTUs 12–17 are most similar to *Synechococcus* P1 and to sequences previously detected only in mats surrounding the YNP cones (Lau *et al.*, 2005). In contrast to the previous report, we detected at least some of these OTUs in cones (e.g., OTU 12, 13). Other unicellular OTUs (25–27) were similar to *Synechococcus* sp. clone JulG-B6 and *Synechocystis* (OTU 7, 8), and were present in both mats and cones.

All major cyanobacterial clusters from 2009 were also represented by 16S rRNA sequences detected in five

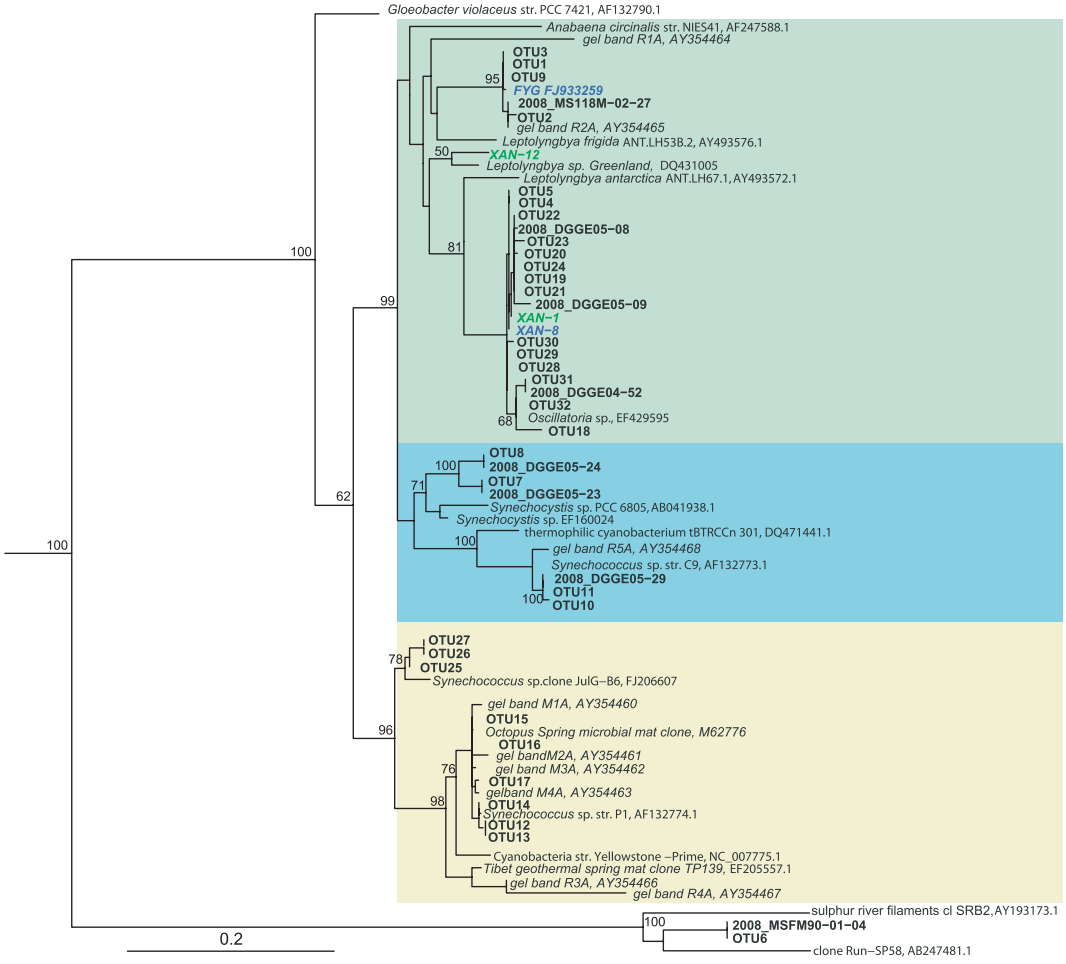


**Fig. 5** Operational taxonomic units (OTUs) of cyanobacteria and environmental samples from coniform mats in Yellowstone National Park (YNP) were inserted into pre-established phylogenetic tree of full-length 16S rRNA gene sequences in Greengenes database in ARB. Numbers on branches indicate bootstrap values obtained by RAxML. Sequences from denaturing gradient gel electrophoresis (DGGE) bands were grouped at 97% sequence similarity threshold. Sequences from enrichment cultures were left as unique sequences. Green and blue text represents sequences of cyanobacteria that do or do not form cones, respectively, in laboratory enrichment cultures. Boldface OTU# represents cyanobacterial sequences from samples collected in 2009, whereas 2008_MS and DGGE sequences represent sequences from samples collected in 2008. Italicized text (*gel band*) are cyanobacterial sequences previously identified in coniform mats (Lau *et al.*, 2005). Accession numbers of GenBank entries are listed after the names of the corresponding organisms, gel bands or clones. Yellow panel denotes *Synechococcus*-like sequences, green panel denotes filamentous *Leptolyngbya*-like cluster, and blue panel denotes unicellular sequences similar to *Synechocystis*. Only bootstrap values larger than 50% are shown.

samples of cones and mats from one pond fed by Mound Spring in 2008 (Fig. 5). The samples from 2008 contained sequences from the larger Subsection III cluster, one sequence from the smaller Subsection III cluster and three sequences similar to those of unicellular cyanobacteria from Subsection I (Fig. 5). However, none of the field samples from 2008 contained the co-occurring OTU 20, 21, 23, 24, although these OTUs were present in all examined ponds in 2009 (including Mound Spring). Furthermore, unicellular sequences were detected only in one of five mats sampled in 2008. Therefore, similar core cyanobacterial clusters contributed to the growth of cones in 2008 and 2009, but individual sequences representing these clusters in Mound Spring varied between the 2 years. Factors responsible for these variations remain unknown and may include both lower temperatures of some ponds in Mound Spring in 2009 (Tables 1 and 2), and different hydrological conditions in Mound Spring between 2008 and 2009 (Table 1).

## Cyanobacterial activity in cones and surrounding mats

To quantify the differential accumulation of biomass in mats and cones, we examined the photosynthetic activity at the approximately 100-μm scale using microelectrodes. The highest net photosynthetic rates in coniform mats occurred in the upper 0.5 mm of the cones (Fig. 7). The ratio of respiration to gross photosynthesis was

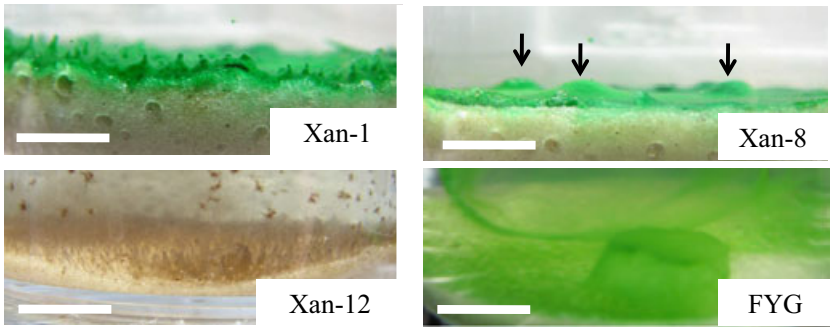


**Fig. 6** Vertical aggregation in enrichment cultures of motile filamentous cyanobacteria from YNP. Vertical structures in the cultures of XAN-1 contain approximately 0.5 mm wide dense central aggregates draped by filmy biofilms on the side. XAN-12 filaments are brown, exhibit possible phycoerhythrin autofluorescence, and form lawns of filmy vertical structures. XAN-8 forms horizontal filmy mats that enclose numerous bubbles (arrows). FYG forms filmy structures and is present in various vertical structures (Bosak *et al.*, 2009, 2010). Scale bar: 4 mm.

$0.91 \pm 0.08$ ($N = 3$) in the upper 0.5 mm of the cones and $1.03 \pm 0.02$ ($N = 3$) in other regions, pointing to more vigorous organic degradation in the interiors of cones and mats. To further link these variations to the activities and densities of individual cyanobacterial cells in cones and mats, we conducted labeling experiments using inorganic carbon and nano-scale Secondary Ion Mass Spectroscopy (NanoSIMS) imaging. The use of $^{13}$C-labeled bicarbonate as a carbon source identified active primary producers and tracked their distribution and densities in different parts of coniform mats (see Fig. S2 for an example of the data).

As indicated by the TEM analyses, both filamentous and sausage-shaped cyanobacteria contained inclusion bodies that likely represent some form of carbon concentrating granules (Fig. 3C,D). Indeed, after a 30-min incubation with $^{13}$C-bicarbonate, these granules were the most prominent loci containing detectable labeled carbon in the uppermost 120 μm of the cone (Fig. 4A). Some label was also present in the filament sheaths at 130 μm below the cone tip (Fig. S7A), but was absent from most other filamentous and sausage-shaped cells in the cone and in the mat. The less abundant, round and oval cyanobacterial cells in the mat exhibited a faster response to the influx of carbon than the immediately adjacent filamentous and sausage-shaped cells, because they contained uniformly distributed $^{13}CN^-$ even after 30 min (Fig. 4C). The rather slow response of the abundant filamentous and sausage-shaped cells to the influx of labeled carbon did not reflect the time required to synthesize the carbon concentrating granules, because abundant, morphologically identical granules were present in the cells from untreated and unlabeled samples (Fig. 3C,D).

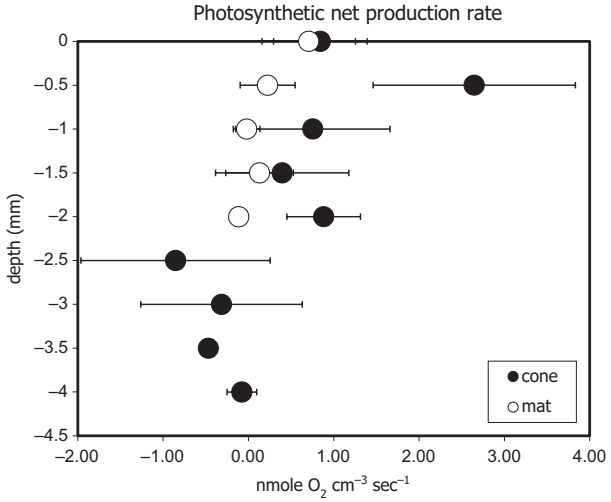


**Fig. 7** Photosynthetic net production rate measurements in cones and mats from YNP. Profiles of net photosynthetic rates (average, $N = 3$) in the top 4 mm of cones and top 2 mm of the adjacent mats. All measurements were performed between 11 am–2 pm in September 2008 and late August 2009 at the light intensity of approximately 1500 μE $m^{-2}$ $s^{-1}$. The photosynthetic rate in cones is nearly constant from 11 a.m. until dusk.

After a 60-min incubation, the label was distributed throughout filamentous and elongated cells in cones and mats (Fig. 4B). Most new inorganic carbon was present in the 100-μm-thick region below the uppermost 90-μm layer of the cone (Fig. 8A). The uptake of $^{13}$C between 90 and 150 μm in the cone was 1.5 times higher than the uptake at the very surface, and more than four times higher than the uptake below the top 0.1 mm of the mat (Fig. 8A). This was owing primarily to the large density of active cells, rather than to the higher activity of individual cells in the tip of the cone (Fig. 8B). The uptake of labeled carbon below the surface of the cone decreased with depth (Fig. 8A). This profile arose from the decreasing density of active cells within the upper 500 μm and not from the decreasing activity of individual cells with depth (Fig. 8B, C). Cells in the uppermost 90 μm of the cone departed from this trend, because individual filaments incorporated lower amounts of label and the overall cell density was lower than in the underlying region (Fig. 8B,C).

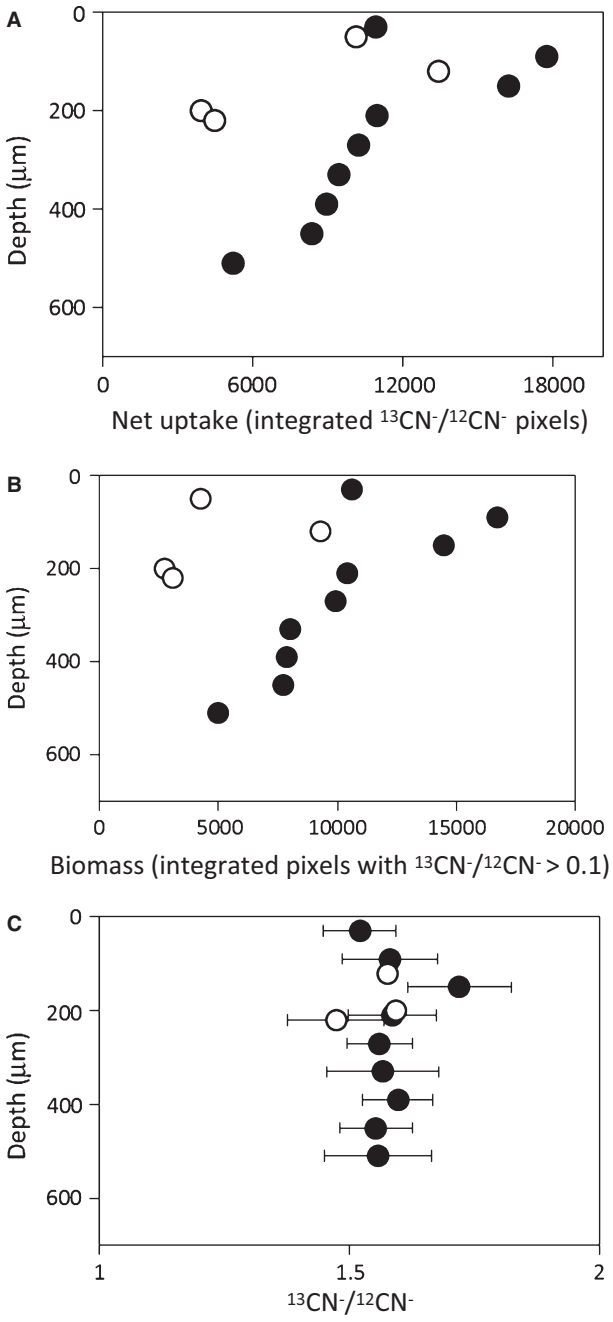


**Fig. 8** Uptake profiles of labeled carbon in a cone and a mat as a function of depth. Data points from the cone are indicated by black circles and those from the mat are indicated by open circles. The uptake of labeled carbon was determined using high-resolution Nano-SIMS on a 60 μm × 60 μm, 256 × 256 pixels survey map (see Fig. S2 for examples). (A) Integrated pixel values of in cones and adjacent mat as a proxy for the net uptake of carbon. Only pixels with $^{13}CN^-/^{12}CN^-$ values > 1.25% were integrated. (B) Biomass (integrated pixels with $^{13}CN^-/^{12}CN^-$values > 0.1) in the cone and the mat. (C) Profile of average $^{13}CN/^{12}CN^-$ ratios in individual filaments ($N$ = 10–30 cells per data point) from the tip to the interior of the cone and the mat ($N$ = 3 cells per data point, where the section allowed recognition of enough filaments).

All parts of mat contained less cellular biomass than the cone and the amount of labeled carbon in cells in the mat decreased with depth, with the possible exception of the very surface (Fig. 8A,B). Active round cells (Fig. 4D) accounted for the threefold increase in the amount of labeled carbon and biomass at approximately 100 μm below the surface (Fig. 8A,B), but similar cells were rare in another isotopically examined mat from the same pond incubated for 30 min. Thus, the topographic lows were laterally heterogeneous, supported smaller active populations of cyanobacteria and exhibited visual and chemical evidence of organic degradation and heavy silicification (Figs 1, 7 and S1–S3).

## DISCUSSION

### Microbial communities in cones and mats

The shapes and the internal textures of modern conical microbialites ultimately preserve little information of the instantaneous molecular diversity and the complexity of microbial interactions. These interactions, however, ensure the persistence of stromatolite-forming communities over timescales necessary to attain macroscopic sizes and turn to rock. Our study reveals a previously unrecognized and spatiotemporally variable composition of cyanobacterial communities in coniform mats in YNP, demonstrates different cellular activities in topographic highs and lows, and hints at factors responsible for the persistence of coniform mats over seasonal and yearly timescales. The molecular diversity of these cyanobacteria varies among cones and mats within the same pond, among different ponds and hot springs (Table 2), and between two successive sampling years (Fig. 5). In the broadest sense, these findings are consistent with the previous reports of morphologically similar filamentous cyanobacteria in cones and mats (Walter *et al.*, 1976; Brock, 1978; Cady & Farmer, 1996; Jones *et al.*, 1998, 2002), and of morphologically more diverse cyanobacteria in the mats (Walter *et al.*, 1976; Brock, 1978). Unlike previous studies, the findings presented here suggest that cyanobacteria responsible for the formation of cones in YNP cannot be described as a single species (Walter *et al.*, 1976), characterized by a single 16S rRNA sequence from Subsection III (Lau *et al.*, 2005), or by an unchanging group of cyanobacterial 16S rRNA sequences (Lau *et al.*, 2005).

Cyanobacterial 16S rRNA sequences from coniform mats around four different hot springs in Sentinel Meadows in 2009, a single hot spring sampled in 2008 and 2009, and from another thermal area (Lau *et al.*, 2005) form clusters. As a whole, these clusters are well represented across space and time. However, the diversity of sequences within individual clusters and samples may, in part, depend on the hydrological conditions. These

conditions would stress communities in ponds with oscillating or rather low temperatures (Tables 1 and 2) and communities in temporarily exposed mats (Rothrock & Garcia-Pichel, 2005). Coniform mats are generally absent from ponds colder than approximately 30 °C and warmer than approximately 55 °C (e.g., Walter *et al.*, 1976; Jones *et al.*, 2002) and *Synechococcus*-like unicells are the dominant cyanobacterial ecotypes above approximately 48 °C (Ferris & Ward, 1997). Therefore, one may expect different cyanobacterial populations in coniform mats exposed to temperatures below 30 °C and above 45 °C than in coniform mats growing permanently within this temperature range. Our current dataset does not support statistically significant relationships of any OTUs with temperature within the observed range (22–51 °C). Some possible differences among samples at the lower and the higher end of this temperature range include the presence of three unique OTUs from Subsection III in the coldest pond (Table 2), the absence of cone-specific and ubiquitous OTU1 at the lowest and the highest temperatures, respectively, and the absence of otherwise ubiquitous OTUs 20, 21, 23, 24 from the warmest pond (Table 2, Fig. S5). At present, these differences remain speculative because the dataset contains samples from only one pond below 30 °C and from only one pond above 47 °C, respectively. Analyses of more samples from temperatures higher than 48 °C and lower than 30 °C, and from more hydrologically stable hot springs elsewhere in YNP could test these suggested trends in a statistically meaningful manner.

The sampling and processing methods used here average the cyanobacterial diversity over entire cones and entire mats, painting a picture in which cyanobacteria with similar or identical 16S rRNA sequences exhibit measurable topography-dependent differences in growth, activity and aggregation (Figs 8 and S6). This picture is consistent with laboratory observations of cone formation in the cultures of filamentous cyanobacteria that were enriched from field cones (XAN-1 and XAN-12 in Fig. 6). These cyanobacteria grow at different rates in cone tips, between mm- to cm-tall cones and on cone sides (Petroff *et al.*, 2011), giving rise to laminated pinnacles in highly enriched laboratory cultures. Other thin and motile filamentous cyanobacteria enriched from field cones appear to be incapable of initiating cone formation under identical growth conditions (XAN-8 in Fig. 6), although their 16S rRNA sequences are very similar to those of known cone formers (XAN-1) and various field OTUs (Fig. 5). Therefore, the diversity of field OTUs likely reflects a number of cyanobacteria capable of cone formation, as well as some that cannot initiate this process but can aggregate into rather flat, tightly woven mats (XAN-8 in Fig. 6), or into thin tubular structures and finely woven floating films (FYG in Fig. 6, after 'filamentous yellow glider', Bosak *et al.*, 2009, 2010). These organisms may contribute to the complex morphologies of coniform mats in the field, which often include filmy, draping, laminated bridges.

Three 'filamentous' cyanobacterial OTUs from YNP cones are cone-specific and one 'unicellular' OTU is mat-specific, suggesting that some cyanobacteria are uniquely adapted to microenvironments within macroscopic cones and mats. Adaptations to the varying intensities and qualities of light and different aggregation behaviors also may underpin the diversity of the four co-occurring OTUs found in many, but not all, cones and mats (OTU 20, 21, 23, 24). Alternatively, this diversity may arise from random fluctuations within the rapidly growing thin layers (Figs 7 and 8) that maintain sectors populated by like individuals even when these individuals carry neutral mutations (Hallatschek & Nelson, 2010; Mitri *et al.*, 2011). Given that 16S rRNA sequences are but a limited measure of the underlying genetic and the physiological diversity (e.g., Moore *et al.*, 1998; Ward *et al.*, 2006), the differences among cyanobacteria from Subsection III in coniform mats may be better resolved by examining longer 16S rRNA sequences, amplifying various functional genes, and analyzing the distribution of OTUs at finer spatial scales within cones and mats.

Thin filamentous cyanobacteria are commonly thought to be *conditio sine qua non* for the formation of cones, but these structures also contain metabolically active and abundant unicellular cyanobacteria (Figs 4 and 5) and thin filaments that may belong to *Chloroflexus*- and *Roseiflexus*-like photosynthetic bacteria (Figs 4E and S4). Our analyses do not identify any of the unicellular cyanobacterial OTUs as cone-specific, in contrast to previous suggestions (Lau *et al.*, 2005). Instead, these OTUs vary among hot springs, ponds, among samples from individual ponds and in time (Figs 5 and S6). This variation may arise as a result of the occasional colonization of coniform surfaces by cyanobacteria from other areas in hot springs. These colonizers may form patchily distributed small populations (Papke & Ward, 2004). The common occurrence of sausage-shaped cyanobacteria in old, decaying coniform mats in the laboratory further points to the ability of these organisms to grow when cone-forming filamentous cyanobacteria do not. Different abundances of individual unicellular OTUs are thus to be expected in actively growing, lithifying, or decaying coniform mats. Samples from more points in time and space would also help distinguish organisms that actively shape coniform mats from organisms that colonize previously formed topography, but are unable to either initiate or maintain cones and the depressions between cones over longer timescales. Such colonization may account for the abundance of sausage-shaped cells in the tips of lightly submerged cones sampled in Mound Spring in 2009 (Fig. 3D), given that mainly thin filamentous cyanobacteria could be identified in the tips of fully

submerged cones from Mound Spring sampled in 2008 (Fig. 3B).

Thin filaments of *Chloroflexus*- or *Roseiflexus*-like organisms are commonly seen in field cones (Fig. 4E), but are generally absent from laboratory cultures. When growing in cyanobacterial mats, these organisms can be photoheterotrophic or photoautotrophic (e.g., van der Meer *et al.*, 2003, 2005) and can contribute to the formation of laminae (Doemel & Brock, 1974). Their contribution to the uptake of inorganic carbon in YNP cones is thought to be small (Walter *et al.*, 1976; Brock, 1978). Indeed, NanoSIMS maps and the accompanying TEM images reveal little labeled carbon in the thin filaments in field cones, even when these filaments are surrounded by highly enriched cyanobacterial cells (Fig. S4). Thin filamentous phototrophs are thus not the main loci of primary production during the main photosynthetic period, but our current data cannot distinguish between their slow autotrophy and photoheterotrophic uptake of labeled cyanobacterial exudates produced during the 60-min incubation. Metabolic potential and function of these thin filaments in coniform mats can be probed in more detail by tracking the distribution of labeled carbon over longer times through high-resolution ultrastructural and NanoSIMS maps (Fig. S4B,C). These measurements should be accompanied by measurements of bulk dissolved organic carbon and $^{13}$C-labeled glycolate and should be conducted at different times of day, including periods of low light (van der Meer *et al.*, 2005).

### Carbon uptake and cone growth

Measurements of $^{13}CN^-$ allow comparisons of the uptake of inorganic carbon among different cells within the same layer of the mat. This method underestimates the rate of the uptake of inorganic carbon because it does not account for the supply of $^{12}CN^-$ produced by the remineralization of unlabeled organic material. However, the recycling of carbon should not affect the observed relationship between cell densities and the position in the mat (Petroff *et al.*, 2011). Field cones (Fig. 8) and laboratory-grown cones (Petroff *et al.*, 2011) exhibit similar profiles of the uptake of carbon with depth. These profiles match the model predictions for biofilms whose growth is limited by the diffusion of nutrients from the overlying stratified solution (Petroff *et al.*, 2011). This model predicts the highest density of active cells in cone tips, because these areas are the closest to the overlying source of nutrients (or light) and are curved. More filaments thus compete for nutrients (or light) in areas of high cell density (cone tips). The YNP cones, which grow at high light intensities (>1500 μE $m^{-2}$ $s^{-1}$), depart from the light-limited or nutrient-limited model in the uppermost approximately 100-μm-thick layer (Fig. 8A). This region contains fewer cells and individual filaments there take up less carbon than those in the dense active layer below the upper 100 μm. In contrast, the uptake of labeled carbon in laboratory cones grown at 200 μE $m^{-2}$ $s^{-1}$ is the highest at the very surface (Petroff *et al.*, 2011). The somewhat lower activity of filaments at the surface of field cones may be attributed to photorespiration and the faster recycling of organic carbon, but it does not support the migration of light-limited growth phototactic cyanobacteria toward topographic highs (Walter *et al.*, 1976). Because the very tip contains few degraded cells and ghosts, the faster recycling of carbon in this region should stem primarily from the microbial degradation of extracellular substances and photorespiration (Bateson & Ward, 1988), rather than from the lysis of inactive cells.

Small-scale isotopic labeling and mapping reveals differences in cyanobacterial responses to the influx of inorganic carbon and nitrogen, potentially limiting nutrients within YNP cones (Wiegert & Fraleigh, 1972; Jahnke *et al.*, 2004; Lolacono *et al.*, 2012). Not only are filamentous cyanobacteria in cones able to extend across diffusive gradients and access nutrients in the overlying solution, but these organisms in cones and mats also concentrate carbon and nitrogen in approximately 300–750 nm large granules (e.g., polysaccharides or cyanophycin). The ability to concentrate carbon and nitrogen may confer an advantage during growth under nutrient-limiting conditions (Shibata *et al.*, 2001; McGinn *et al.*, 2003). The large round photosynthetic cells below the surface of the horizontal mats respond to the influx of carbon and nutrients faster than the filamentous and sausage-shaped cyanobacteria, have a laterally discontinuous distribution, and occur below the upper 150 μm of the mat. These observations suggest that the oval cells grow sporadically during nutrient pulses and are adaptated to lower light intensities. Our current experiments track the initial incorporation and distribution of labeled inorganic carbon in the cells of primary producers, but do not determine the longer-term fate of the newly synthesized organic carbon. The latter may critically influence the preservation of coniform mats and their robustness because the abundance of excreted substances (i.e., extracellular biomass) may distinguish the sturdy, cohesive cones in the field from the often filmy, internally porous, transparent structures in the highly enriched laboratory cultures (Fig. 6). The extracellular compounds contain less nitrogen and sulfur relative to cellular biomass and, with the possible exception of cyanobacterial sheaths (Fig. S7), may not be detectable as $CN^-$ ions by NanoSIMS (Figs 4 and S2). Future studies can investigate these processes by following the production and distribution of new cellular biomass and exopolymeric substances, the flow of carbon from primary producers to other organisms, and total microbial diversity in coniform mats.

### Growth and preservation of cones by silicification

The topography-dependent and temporally variable growth of coniform mats in modern hot springs leads to the formation of porous and dense laminae, textural differences between cones and mats, and distinct macroscopic topography. Cones contain more porous laminae formed by filaments that are oriented randomly or are perpendicular with respect to the growth surface. Recent studies report that these orientations occur primarily in actively photosynthesizing, diffusion-limited mats (Petroff *et al.*, 2010). Structures that form under light-limited conditions, where diffusion limitation should be less pronounced, contain thin, dense laminae of mutually aligned prostrate filaments (Bosak *et al.*, 2009). Thus, the higher availability of nutrients at cone tips in stratified solutions (Jorgensen & DesMarais, 1990) and the depletion of these nutrients within the mat (Petroff *et al.*, 2011) may promote the growth of cone tips and lead to the formation of porous laminae characterized by less abundant cells and more abundant exopolymeric substances (Fig. S7). Textural record of these topography-dependent and time-dependent processes can be preserved by precipitating silica. In some flat laminated microbialites, actively growing microbes outpace silicification, giving rise to porous laminae encrusted by silica, whereas biomass-poor and silica-rich laminae form in autumn/winter when the growth is slow and microbes are unable to outpace silicification (Konhauser *et al.*, 2001, 2004). In keeping with this model, the sparse and more heavily encrusted cells in the topographic lows of coniform mats may be attributed to the slower accumulation of biomass in topographic lows relative to mineral precipitation. Conversely, the fast accumulation of biomass in actively growing cone tips outpaces mineral precipitation and results in unmineralized or only lightly mineralized cells. These preservational mechanisms in coniform mats can give rise not only to the alternating cell-rich and cell-poor laminae driven by seasonal variations in growth, as is the case in stratiform microbialites (Konhauser *et al.*, 2001), but also to the laminae produced by the more rapidly varying orientation of cyanobacterial filaments in cones (e.g., Walter *et al.*, 1976; Petroff *et al.*, 2010). All cones shown and analyzed in this study were, at best, lightly mineralized, and their fine organic laminae may not be preserved by silicification. This does not diminish the value of these coniform mats as model systems in which to study biological aspects of stromatolite morphogenesis, as faster silicification has the potential to preserve small-scale textures in cones from some less accessible localities in YNP (e.g., Fig S3A–C in Bosak *et al.*, 2009). A more critical difference between modern coniform mats and ancient conical stromatolites is mineralogical: most modern small cones are preserved by silicification, but ancient cones were preserved primarily by calcium carbonate. Therefore, direct insights into stromatolites as records of past chemical conditions and possible influences of microbial metabolisms on carbonate precipitation require more studies of the growth and preservation of coniform mats in carbonate-precipitating environments.

## CONCLUSIONS

Filamentous cyanobacteria build the vertical scaffolding of conical microbialites that grow in the shallow pools of modern alkaline hot springs. These organisms are present throughout the cones and the adjacent horizontal mats, and most of their 16S rRNA gene sequences are not specific to either cones or mats. Field sequences of filamentous cyanobacteria in coniform mats belong to two principal clusters and have cultured representatives that form vertical structures in highly enriched laboratory cultures. Cyanobacterial sequences vary among different hot springs, among ponds in the same hot spring, and even in one location between two sampling years. Therefore, the growth of modern conical microbialites depends on a number of genetically distinct filamentous cyanobacteria rather than a single organism or an unchanging group of organisms. Unicellular sequences in coniform mats vary even among samples from the same pond and are often undetectable, although photosynthetically active *Synechococcus*-like cyanobacteria are present in cones. Most new cellular biomass in cones grows in the tips, but not at the very surface. In mats, the very surface is both the densest and the most active growth layer, while organic degradation is prevalent in the mat interior. There, cyanobacteria in hot spring coniform mats morphologically diverse and photosynthetically active unicellular cyanobacteria quickly respond to nutrient pulses, but are unable to extend across diffusive gradients and form cohesive porous laminae.

## ACKNOWLEDGMENTS

We thank G. Geesey (U. Montana), S. Gunther (NPS), J. Thompson (MIT), L. Casillas (Univ. PR), D. Newman Lab (MIT), J. Holz and N. Watson (Keck Biological Imaging Facility, Whitehead Institute, MIT), members of the MIT Laboratory for Geomicrobiology and Microbial Sedimentology and Dr. S. K. Sears (McGill Univ.). H.V. acknowledges financial support from the Natural Sciences and Engineering Research Council (NSERC) of Canada. We also thank the PICT-IBiSA imaging facility in the Institut Curie for NanoSIMS analyses. Thoughtful comments by three anonymous reviewers improved the manuscript.

## REFERENCES


Agresti A (1990) *Categorical Data Analysis*. John Wiley & Sons, Inc., Hoboken, NJ, USA.

Altschul SF, Madden TL, Schaffer AA, Zhang J, Zhang Z, Miller W, Lipman DJ (1997) Gapped BLAST and PSI-BLAST: a new generation of protein database search programs. *Nucleic Acids Research* **25**, 3389–3402.

Bartley JK, Grotzinger JP, Knoll AH, Sergeev VN (2000) Lithification and fabric genesis in precipitated stromatolites and associated peritidal carbonates, Mesoproterozoic Billyakh Group, Siberia. In *Carbonate Sedimentation and Diagenesis in the Evolving Precambrian World* (eds Grotzinger JP, James NP). SEPM Special Publications, Tulsa, OK, pp. 59–73.

Bateson MM, Ward DM (1988) Photoexcretion and fate of glycolate in a hot spring cyanobacterial mat. *Applied and Environment Microbiology* **54**, 1738–1743.

Benson D (2003) HSI ratio method. Multi-Isotope Imaging Mass Spectrometry Workshop, Cambridge, Massachusetts, http://www.nrims.harvard.edu/slides/NRIMS_-_BensonWorkshop2003.pdf.

Beukes NJ, Lowe DR (1989) Environmental controls on diverse stromatolite morphologies in the 3000 Myr Pongola Supergroup, South Africa. *Sedimentology* **36**, 383–397.

Boomer SM, Noll KL, Geesey GG, Dutton BE (2009) Formation of multilayered photosynthetic biofilms in an alkaline thermal spring in Yellowstone National Park, Wyoming. *Applied and Environment Microbiology* **75**, 2464–2475.

Bosak T, Liang B, Sim MS, Petroff APP (2009) Morphological record of oxygenic photosynthesis in conical stromatolites. *Proceedings of the National Academy of Sciences of the USA* **106**, 10939–10943.

Bosak T, Bush J, Flynn M, Liang B, Ono S, Petroff APP, Sim MS (2010) Formation and stability of oxygen-rich bubbles that shape photosynthetic mats. *Geobiology* **8**, 45–55.

Brock TD (1978) *Thermophilic Microorganisms and Life at High Temperatures*. Springer-Verlag, Berlin, Germany, pp 465.

Buick R (1992) The antiquity of oxygenic photosynthesis: evidence from stromatolites in sulphate-deficient Archaean lakes. *Science* **255**, 74–77.

Burton S, Lee J (1978) Improved enrichment and isolation procedures for obtaining pure cultures of Beggiatoa. *Applied and Environment Microbiology* **35**, 614–617.

Cady SL, Farmer JD (1996) Fossilization processes in siliceous thermal springs: trends in preservation long thermal gradients. In: *Evolution of Hydrothermal Ecosystems on Earth (and Mars?)* (eds Bock GR, Goode JA). John Wiley & Sons Ltd, Chichester, pp. 150–173.

Cannon GC, Bradburne CE, Aldrich HC, Baker SH, Heinhorst S, Shively JM (2001) Microcompartments in Prokaryotes: Carboxysomes and related polyhedra. *Applied and Environment Microbiology* **67**, 5351–5361.

Castenholz RW (1988) *Cyanobacteria*. Academic Press, San Diego.

Castenholz RW (2001) Cyanobacteria. In: *Bergey's Manual of Systematic Bacteriology*, 2nd edn, Vol. 1, (eds Boone DR, Castenholz RW, Garrity GM) The Archaea and the Deeply Branching and Phototrophic Bacteria. Springer Verlag, NY. pp. 473-599.

Davis JP, Youssef NH, Elshahed MS (2009) Assessment of the diversity, abundance, and ecological distribution of members of candidate division SR1 reveals a high level of phylogenetic diversity but limited morphotypic diversity. *Applied and Environment Microbiology* **75**, 4139–4148.

DeSantis TZ, Hugenholtz N, Larsen N, Rojas M, Brodie EL, Keller K, Huber T, Dalevi D, Hu P, Andersen G (2006a) Greengenes, a Chimera-Checked 16S rRNA Gene Database and Workbench Compatible with ARB. *Applied and Environment Microbiology* **72**, 5069–5072.

DeSantis TZ Jr, Hugenholtz P, Keller K, Brodie EL, Larsen N, Piceno YM, Phan R, Andersen GL (2006b) NAST: a multiple sequence alignment server for comparative analysis of 16S rRNA genes. *Nucleic Acids Research* **34**, W394–W399.

Doemel WN, Brock TD (1974) Bacterial stromatolites: origins of laminations. *Science* **184**, 1083–1086.

Ferris MJ, Ward DM (1997) Seasonal distributions of dominant 16S rRNA-defined populations in a hot spring microbial mat examined by denaturing gradient gel electrophoresis. *Applied and Environment Microbiology* **63**, 1375–1381.

Ferris MJ, Kuhl M, Wieland A, Ward DM (2003) Cyanobacterial ecotypes in different optical microenvironments of a 68° C hot spring mat community revealed by 16S-23S rRNA internal transcribed spacer region variation. *Applied and Environment Microbiology* **69**, 2893–2898.

Foster JS, Green SJ, Ahrendt SR, Golubic S, Reid RP, Hetherington KL, Bebout L (2009) Molecular and morphological characterization of cyanobacterial diversity in the stromatolites of Highborne Cay, Bahamas. *ISME Journal* **3**, 573–587.

Grey K (1980) Small conical stromatolites from the Archean near Kanowna, Western Australia. Annu Report Geol Surv Western Australia, Perth, pp. 90–94.

Grotzinger JP, Knoll AH (1999) Stromatolites in Precambrian carbonates: evolutionary mileposts or environmental dipsticks? *Annual Review of Earth and Planetary Sciences* **27**, 313–358.

Grotzschel S, de Beer D (2002) Effect of oxygen concentration on photosynthesis and respiration in two hypersaline microbial mats. *Microbial Ecology* **44**, 208–216.

Guerquin-Kern JL, Wu TD, Quintana C, Croisy A (2005) Progress in analytical imaging of the cell by dynamic secondary ion mass spectrometry (SIMS microscopy). *Biochimica et Biophysica Acta* **1724**, 228–238.

Hallatschek O, Nelson DR (2010) Life at the front of an expanding population. *Evolution* **64**, 193–206.

Hanada S, Takaichi S, Matsuura K, Nakamura K (2002) *Roseiflexus castenholzii* gen. nov., sp. nov., a thermophilic, filamentous, photosynthetic bacterium that lacks chlorosomes. *International Journal of Systematic and Evolutionary Microbiology* **52**, 187–193.

Hofmann HJ, Jackson GD (1987) Proterozoic ministromatolites with radial-fibrous fabric. *Sedimentology* **34**, 963–971.

Huber T, Faulkner G, Hugenholtz P (2004) Bellerophon: a program to detect chimeric sequences in multiple sequence alignments. *Bioinformatics* **20**, 2317–2319.

Jahnke LL, Embaye T, Hope J, Turk KA, Van Zuilen M, Des Marais DJ, Farmer JD, Summons RE (2004) Lipid biomarker and carbon isotopic signatures for stromatolite-forming, microbial mat communities and *Phormidium* cultures from Yellowstone National Park. *Geobiology* **2**, 31–47.

Jones B, Renaut RW, Rosen MR (1998) Microbial biofacies in hot-spring sinters; a model based on Ohaaki Pool, North Island, New Zealand. *Journal of Sedimentary Research* **68**, 413–434.

Jones E, Oliphant T, Peterson P (2001) SciPy: open source scientific tools for Python. http://www.scipy.org/ (accessed on 6 June 2012).

Jones B, Renaut RW, Rosen MR, Ansdell KM (2002) Coniform stromatolites from geothermal systems, North Island, New Zealand. *Palaios* **17**, 84–103.

Jorgensen BB, DesMarais DJ (1990) The diffusive boundary layer of sediments: oxygen microgradients over a microbial mat. *Limnology and Oceanography* **35**, 1343–1355.

Jorgensen BB, Revsbech NP (1985) Diffusive boundary-layers and the oxygen-uptake of sediments and detritus. *Limnology and Oceanography* **30**, 111–122.

Kah LC, Knoll AH (1996) Microbenthic distribution of Proterozoic tidal flats: environmental and taphonomic considerations. *Geology* **24**, 79–82.

Konhauser KO, Phoenix VR, Bottrell SH, Adams DG, Head IM (2001) Microbial-silica interactions in Icelandic hot spring sinter: possible analogues for some Precambrian siliceous stromatolites. *Sedimentology* **48**, 415–433.

Konhauser KO, Jones B, Phoenix VR, Ferris G, Renaut RW (2004) The microbial role in hot spring silicification. *Ambio* **33**, 552–558.

Lacap DC, Smith GJD, Warren-Rhodes K, Pointing SB (2005) Community structure of free-floating filamentous cyanobacterial mats from the Wonder Lake geothermal springs in the Philippines. *Canadian Journal of Microbiology* **51**, 583–589.

Lacap DC, Barraquio W, Pointing SB (2007) Thermophilic microbial mats in a tropical geothermal location display pronounced seasonal changes but appear resilient to stochastic disturbance. *Environmental Microbiology* **9**, 3065–3076.

Lane DJ (1991) 16S/23S rRNA sequencing. In *Nucleic Acid Techniques in Bacterial Systematics* (eds Stackebrandt E, Goodfellow M). John Wiley and Sons, Chichester, UK, pp. 115–175.

Lassen C, Glud RN, Ramsing NB, Revsbech NP (1998) A method to improve the spatial resolution of photosynthetic rates obtained by oxygen microsensors. *Journal of Phycology* **34**, 89–93.

Lau E, Nash CZ, Vogler DR, Cullings KW (2005) Molecular diversity of cyanobacteria inhabiting coniform structures and surrounding mat in a Yellowstone hot spring. *Astrobiology* **5**, 83–92.

Legendre P, Legendre L (1998) *Numerical Ecology*. Elsevier, Amsterdam, pp 870.

Lolacono ST, Meyer-Dombard DR, Havig JR, Poret-Peterson AT, Hartnett HE, Shock EL (2012) Evidence for high temperature in situ nif transcription in an alkaline hot spring of the Lower Geyser Basin, Yellowstone National Park. *Environmental Microbiology*, doi:10.1111/j.1462-2920.2012.02710.x.

Ludwig W, Strunk O, Westram R, Richter L, Meier H, Yadhukumar, Buchner A, Lai T, Steppi S, Jobb G, Forster W, Brettske I, Gerber S, Ginhart AW, Gross O, Grumann S, Hermann S, Jost R, Konig A, Liss T, Lussmann R, May M, Nonhoff B, Reichel B, Strehlow R, Stamatakis A, Stuckmann N, Vilbig A, Lenke M, Ludwig T, Bode A, Schleifer KH (2004) ARB: a software environment for sequence data. *Nucleic Acids Research* **32**, 1363–1371.

McGinn PJ, Price GD, Maleszka R, Badger MR (2003) Inorganic carbon limitation and light control the expression of transcripts related to the $CO_2$-concentrating mechanism in the cyanobacterium *Synechocystis* sp. strain PCC6803. *Plant Physiology* **132**, 218–219.

McGregor GB, Rasmussen JP (2008) Cyanobacterial composition of microbial mats from an Australian thermal spring: a polyphasic evaluation. *FEMS Microbiology Ecology* **63**, 23–35.

van der Meer MTJ, Schouten S, Sinninghe Damsté J, de Leeuw JW, Ward DM (2003) Compound-specific isotopic fractionation patterns suggest different carbon metabolisms among *Chloroflexus*-like bacteria in hot-spring microbial mats. *Applied and Environment Microbiology* **69**, 6000–6006.

van der Meer MTJ, Schouten S, Bateson MM, Nübel U, Wieland A, Kühl M, de Leeuw JW, Sinninghe Damsté J, Ward DM (2005) Diel variations in carbon metabolism by green nonsulfur-like bacteria in alkaline siliceous hot spring microbial mats from Yellowstone National Park. *Applied and Environment Microbiology* **71**, 3978–3986.

Mitri S, Xavier JB, Foster KR (2011) Social evolution in multispecies biofilms. *Proceedings of the National Academy of Sciences of the USA* **108**, 10839–10846.

Moore LR, Rocap G, Chisholm SP (1998) Physiology and molecular phylogeny of coexisting *Prochlorococcus* ecotypes. *Nature* **393**, 464–467.

Nash A (1938) The Cyanophyceae of the thermal regions of Yellowstone National Park, U.S.A., and of Rotorua and Whakarewarewa, New Zealand; with some ecological data. Ph. D. Thesis, University of Minnesota, Minneapolis, MN, pp. 220.

Nubel U, Garcia Pichel F, Muyzer G (1997) PCR primers to amplify 16S rRNA genes from cyanobacteria. *Applied and Environment Microbiology* **63**, 3327–3332.

Papke RT, Ward DM (2004) The importance of physical isolation to microbial diversification. *FEMS Microbiology Ecology* **48**, 293–303.

Petroff APP, Sim MS, Maslov A, Krupenin M, Rothman DH, Bosak T (2010) Biophysical basis for the geometry of conical stromatolites. *Proceedings of the National Academy of Sciences of the USA* **107**, 9956–9961.

Petroff APP, Wu T-D, Liang B, Mui J, Guerquin-Kern J-L, Vali H, Rothman DH, Bosak T (2011) Reaction-diffusion model of nutrient uptake in a biofilm: theory and experiment. *Journal of Theoretical Biology* **289**, 90–95.

Pierson BK, Castenholz RW (1974) A phototrophic gliding filamentous bacterium of hot springs, *Chloroflexus aurantiacus*, gen. and sp. nov. *Archives of Microbiology* **100**, 5–24.

Pierson BK, Giovannoni SJ, Stahl DA, Castenholz RW (1985) *Heliothrix oregonensis*, gen. nov., sp. nov., a phototrophic filamentous gliding bacterium containing bacteriochlorophyll *a*. *Archives of Microbiology* **142**, 164–167.

Poczatek C, Kauman Z, Lechene CP (2009) OpenMIMS ImageJ Plugin Guide. *Harvard Medical School*, Boston, MA.

Pope MC, Grotzinger JP (2000) Controls on fabric development and morphology of tufas and stromatolites, uppermost Pethei Group (1.8 Ga), Great Slave Lake, northwest Canada. In: *Carbonate Sedimentation and Diagenesis in the Evolving Precambrian World* (eds Grotzinger JP, James NP), SEPM Special Publications, Tulsa, Oklahoma, pp. 103–121.

Rasband WS (1997–2006). *ImageJ*, U. S. National Institute of Health. Bethesda, Maryland, USA.

Revsbech NP (1989) An oxygen microsensor with a guard cathode. *Limnology and Oceanography* **34**, 474–478.

Revsbech NP, Jorgensen BB (1983) Photosynthesis of benthic microflora measured with high spatial resolution by the oxygen microprofile method: capabilities and limitations of the method. *Limnology and Oceanography* **28**, 749–756.

Rothrock MJ, Garcia-Pichel F (2005) Microbial diversity of benthic mats along a tidal desiccation gradient. *Environmental Microbiology* **7**, 593–601.

Semikhatov MA, Gebelein CD, Cloud PE, Awramik SM, Benmore WC (1979) Stromatolite morphogenesis-progress and problems. *Canadian Journal of Earth Sciences* **16**, 992–1015.

Shibata M, Ohkawa H, Kaneko T, Fukuzawa H, Tabata S, Kaplan A, Ogawa T (2001) Distinct constitutive and low-CO2-induced CO2 uptake systems in cyanobacteria: genes involved and their phylogenetic relationship with homologous genes in other organisms. *Proceedings of the National Academy of Sciences of the USA* **98**, 11789–11794.

Stamatakis A, Hoover P, Rougemont J (2008) A rapid bootstrap algorithm for the RAxML web servers. *Systematic Biology* **57**, 758–771.

Vaara T, Vaara M, Niemela S (1979) Two improved methods for obtaining axenic cultures of cyanobacteria. *Applied and Environment Microbiology* **38**, 1011–1014.

Walter MR, Bauld J, Brock TD (1972) Siliceous algal and bacterial stromatolites in hot spring and geyser effluents of Yellowstone National Park. *Science* **178**, 402–405.

Walter MR, Bauld J, Brock TD (1976) Microbiology and morphogenesis of columnar stromatolites (*Conophyton, Vacerrilla*) from hot springs in Yellowstone National Park. In *Developments in Sedimentology, Stromatolites* (ed. Walter MR). Elsevier, Amsterdam, pp. 273–310.

Ward DM, Bateson MM, Ferris MJ, Kuhl M, Wieland A, Koeppel A, Cohan FM (2006) Cyanobacterial ecotypes in the microbial mat community of Mushroom Spring (Yellowstone National Park, Wyoming) as species-like units linking microbial community composition, structure and function. *Philosophical Transactions of the Royal Society of London. Series B, Biological Sciences* **361**, 1997–2008.

Weller D, Doemel W, Brock TD (1975) Requirement of low oxidation-reduction potential for photosynthesis in a blue-green alga (*Phormidium* sp.). *Archives of Microbiology* **104**, 7–13.

Wiegert RG, Fraleigh PC (1972) Ecology of Yellowstone thermal effluent systems: net primary production and species diversity of a successional blue-green algal mat. *Limnology and Oceanography* **17**, 215–228.

## SUPPORTING INFORMATION

Additional Supporting Information may be found in the online version of this article:

**Fig. S1** Lithification in cones and mats.

**Fig. S2** Cone-mat sample (photograph, scale in mm) incubated with labeled carbon for 60 minutes showing the distribution of 60 μm × 60 μm NanoSIMS maps and high resolution maps showing different cell morphologies.

**Fig. S3** NanoSIMS analysis of a cone (A) and a mat (B) incubated for 60 min in labeled inorganic carbon in 2008.

**Fig. S4** Distribution of unlabeled and labeled carbon in thin filaments in the cone incubated with labeled inorganic carbon for 60 min.

**Fig. S5** Spatial distribution of OTUs in the samples of cones and mats from four different springs.

**Fig. S6** Distribution of OTUs in cones and mats from four different springs in 2009.

**Fig. S7** NanoSIMS maps of YNP cones showing possible cyanobacterial sheaths.

Please note: Wiley-Blackwell are not responsible for the content or functionality of any supporting materials supplied by the authors. Any queries (other than missing material) should be directed to the corresponding author for the article.